

Semi-Blind Joint Channel and Symbol Estimation for Beyond Diagonal Reconfigurable Surfaces

Gilderlan Tavares de Araújo, *Member, IEEE*, André L. F. de Almeida, *Senior Member, IEEE*, Bruno Sokal, *Member, IEEE*, Gabor Fodor, *Fellow, IEEE*, Paulo R. B Gomes, *Member, IEEE*

Abstract—The beyond-diagonal reconfigurable intelligent surface (BD-RIS) is a recent architecture in which scattering elements are interconnected to enhance the degrees of freedom for wave control, yielding performance gains over traditional single-connected RISs. For BD-RIS, channel estimation – well-studied for conventional RIS – becomes more challenging due to the complex connections and a larger number of coefficients. Prior works rely on pilot-assisted estimation followed by data decoding. This paper introduces a semi-blind tensor-based approach for joint channel and symbol estimation that eliminates the need for training sequences by leveraging data symbols directly. A practical scenario with time-varying user terminal-RIS channels under mobility is considered. By reformulating the received signal from a tensor decomposition perspective, we develop two semi-blind receivers: a two-stage method transforming the fourth-order PARATUCK model into a third-order PARAFAC model, and a single-stage iterative process based on fourth-order TUCKER decomposition. Identifiability conditions for reliable joint recovery are derived, and numerical results demonstrate the performance advantages and trade-offs of the proposed schemes over existing solutions.

Index Terms—Beyond diagonal RIS, tensor decomposition, semi-blind receivers, PARATUCK, PARAFAC.

I. INTRODUCTION

RECONFIGURABLE surfaces are a promising technology for future wireless communication systems [1]–[3]. Primary attention has been given to the passive reconfigurable intelligent surface (RIS) architecture, equipped solely with reflection capabilities. Recently, new architectures have been intensively studied to address the limitations of the traditional RIS and to enhance system performance. Examples are hybrid RIS architectures [4]–[6] that mitigate the double fading effect and the simultaneously transmitting and reflecting reconfigurable intelligent surface (STAR-RIS) architecture [7]–[9], which supports reflection and transmission capabilities.

A new RIS architecture with a non-diagonal RIS phase shift matrix was recently proposed in [10], [11]. The so-called beyond-diagonal reconfigurable intelligent surface

The authors thank the partial support of FUNCAP under grant ITR-0214-00041.01.00/23, and the National Institute of Science and Technology (INCT-Signals) sponsored by Brazil's National Council for Scientific and Technological Development (CNPq) under grant 406517/2022-3.

Gilderlan T. de Araújo and Paulo. R. B. Gomes are with the Federal Institute of Ceará, e-mails: {gilerlan.tavares,gomes.paulo}@ifce.edu.br.

André L. F. de Almeida and Bruno Sokal are with the Teleinformatics Department, Federal University of Ceará, Fortaleza-CE, e-mail: {andre,brunosokal}@gtel.ufc.br.

G. Fodor was funded by the Swedish Strategic Foundation Future Software Systems Project SAICOM, grant no: FUS21-0004

(BD-RIS) introduces additional degrees of freedom for system optimization, resulting in significant performance improvements compared to conventional diagonal RIS (single-connected, i.e., there are no connections between the RIS elements). The non-diagonal structure of the phase shift matrix also emerges in scenarios involving non-reciprocal connections among RIS elements (e.g., group-connected and fully-connected cases), allowing an incident signal to be reflected by a different element [12]. In [13], a modeling and architecture design based on scattering network analysis was proposed. More recently, [14] introduced a RIS modeling framework grounded in multiport network analysis, while optimization algorithms for BD-RIS were explored in [15], [16]. Despite its potential, this technology faces several challenges, including channel estimation, the joint optimization of passive and active beamforming, and the mitigation of multi-user interference [17].

The promised performance enhancements offered by BD-RIS relative to traditional single-connected RIS depend strongly on the accuracy of the channel state information (CSI). As far as channel estimation is concerned, most efforts have focused on traditional single-connected RIS architectures, where the phase shift matrix is assumed to be diagonal, implying no physical coupling among RIS elements. However, the lack of signal processing capabilities in BD-RIS, combined with its more complex connection structure, makes channel estimation even more challenging than in single-connected RIS. Few solutions have been proposed for channel estimation in BD-RIS. In [11], a least squares (LS) method was introduced to estimate the cascaded channel (base station (BS) to BD-RIS to user terminal (UT) channel). Despite its conceptual simplicity, this method requires a significant training overhead. The authors in [18] proposed closed-form and iterative algorithms for BD-RIS channel estimation, leveraging tensor decomposition techniques. While the approach of [11] only estimates the cascaded channel, the tensor-based methods proposed in [18] provide individual estimates of the involved channel matrices, yielding performance enhancements while significantly reducing training overhead. Nevertheless, these methods rely on pilot sequences, meaning that CSI acquisition and data detection are performed in two consecutive stages. More recently, [19] proposed a semi-blind joint channel and symbol estimation approach for BD-RIS¹. In a

¹This paper corresponds to the conference version of the present work, where a quasi-static user-RIS channel was considered.

MIMO communication scenario, this method directly provides decoupled estimates of the involved channel matrices by leveraging tensor modeling of the received signals via a PARATUCK decomposition [20].

Tensor decompositions are powerful mathematical tools for modeling and estimating the multidimensional structure of signals and data. As demonstrated by extensive signal processing literature, tensor modeling provides a concise and elegant framework for addressing various problems, such as blind/semi-blind channel estimation and data detection in wireless communications [21]–[26]. More recently, tensor-based receiver algorithms have proven to be highly effective in RIS-assisted MIMO communication systems [27], [28]. In the context of single-connected RIS-assisted communications, tensor modeling approaches have been exploited to solve problems such as phase shift optimization [29], feedback overhead reduction [30], and channel estimation [31]–[34]. To the best of our knowledge, semi-blind joint channel and symbol estimation for BD-RIS has not yet been well investigated in the literature. Leveraging useful data symbols for channel estimation avoids the need to transmit lengthy pilot sequences, while using actual information symbols to refine channel estimates. This approach also allows reducing decoding latency, since early detection can be carried out jointly with channel estimates.

This paper considers the problem of semi-blind joint channel and symbol estimation methods for BD-RIS. We are interested in data-driven solutions that yield decoupled estimates of the involved communication channels (UT to BD-RIS and BD-RIS to BS) without a prior dedicated training sequence stage² and that can operate under less restrictive system parameter choices compared to the conventional pilot-assisted LS method. Adopting a novel non-diagonal scattering design for semi-blind channel estimation, where the BD-RIS phase shift matrix is expressed as the product of a scattering matrix and a diagonal rotation matrix, the received signal can be recast as a fourth-order tensor that follows a PARATUCK-based model. By exploiting the resulting algebraic signal structure, we derive two novel receiver algorithms for joint channel and symbol estimation. The first one recasts the received signal tensor as a structured third-order PARAFAC model, from which channel and symbol estimation are carried out in two stages. In the second one, the received signal is reshaped into a fourth-order TUCKER tensor, allowing us to derive a single-stage channel and symbol estimation scheme based on a trilinear alternating least squares (TALS) algorithm. Compared to the conference version in [19], this paper provides a complete formulation of the proposed semi-blind BD-RIS channel estimation problem, presents detailed derivations of the two proposed algorithms, discusses identifiability conditions and their implications to system design, while handling channels that vary at different time scales, accounting for some level of user mobility.

²It is worth noting that the proposed semi-blind receivers can offer higher spectral efficiency and lower data decoding latency compared to pilot-assisted methods, since the decoding of useful transmitted data already happens in the CE stage

Extensive numerical results are also provided for performance evaluation in various setups.

The main contributions of this work can be summarized as follows.

- We propose a data-driven channel estimation approach for BD-RIS, where the separate estimates of the involved channel matrices are obtained without pilot sequences by exploiting a tensor algebraic signal structure based on a PARATUCK-(2,4) decomposition.
- By exploiting two different tensor reshapings of the received signal, we derive two semi-blind receivers. We first formulate a two-stage receiver that yields estimates of the two channel matrices and the symbol matrix in two consecutive stages by recasting the received signal as a structured PARAFAC model. Then, a second receiver is derived that solves the problem of channel and symbol estimation iteratively in a single stage by resorting to a fourth-order TUCKER modeling.
- We study the identifiability conditions for the joint channel and symbol estimation, considering the two proposed receivers. We also discuss the design of the BD-RIS scattering matrix and the computational complexity of the proposed methods. Our study sheds light on the trade-offs between the two proposed receivers, accounting for both complexity and performance.
- Extensive numerical results are provided to evaluate the performance of the proposed semi-blind receivers. Our results show that both algorithms present a good performance. The TUCKER receiver is more efficient than the PAKRON receiver. However, it is more computationally complex. Additionally, we compare our proposed method with the pilot-assisted method, achieving better performance than traditional LS and worse than other tensor methods in composite channel estimation. However, our method is semi-blind, which improves the spectral efficiency compared to both competitor methods.

The remainder of the paper is organized as follows. Section II presents the system model, while Section III details the two proposed receivers. In Section IV, we discuss identifiability and complexity, along with the trade-offs associated with the proposed receivers. Simulation results are provided in Section V, while our concluding remarks are given in Section VI.

Notation and properties: Matrices are represented with boldface capital letters (\mathbf{A}), and vectors are denoted by boldface lowercase letters (\mathbf{a}). Tensors are symbolized by calligraphic letters (\mathcal{A}). Hermitian, Transpose and pseudo-inverse of a matrix \mathbf{A} are denoted as \mathbf{A}^H , \mathbf{A}^T and \mathbf{A}^\dagger , respectively. \mathbf{A}_i and $\mathbf{A}_{.j}$ denotes the i -th row and j -th column of the matrix \mathbf{A} , respectively. $\mathbf{D}_i(\mathbf{A}) = \text{diag}(\mathbf{A}_{.i})$ is a diagonal matrix holding the i -th row of \mathbf{A} on its main diagonal, since the operator $\text{diag}(\mathbf{a})$ forms a diagonal matrix out of its vector argument. \ast , \circ , \diamond , \odot and \otimes denote the conjugate, outer product, Khatri Rao, Hadamard, and Kronecker products, respectively. \mathbf{I}_N denotes the $N \times N$ identity matrix. The operator $\text{vec}(\cdot)$ vectorizes an $I \times J$ matrix argument, while

$\text{unvec}_{I \times J}(\cdot)$ does the opposite operation. Moreover, $\text{vecd}(\cdot)$ forms a vector out of the diagonal of its matrix argument. The n mode product between a tensor $\mathcal{Y} \in \mathbb{C}^{I \times J \dots \times K}$ and a matrix $\mathbf{A} \in \mathbb{C}^{I \times R}$ is denoted as $\mathcal{Y} \times_n \mathbf{A}$, for $1 \leq n \leq N$. An identity N -way tensor of dimension $R \times R \times \dots \times R$ is denoted as $\mathcal{I}_{N,R}$. $\mathbf{1}_{M,N}$ is an $M \times N$ one matrix. \sqcup_n denotes the concatenating operator related to the n -mode. In this paper, we make use of the following identities:

$$\text{vec}(\mathbf{ABC}) = (\mathbf{C}^T \otimes \mathbf{A})\text{vec}(\mathbf{B}). \quad (1)$$

$$\text{diag}(\mathbf{a})\mathbf{b} = \text{diag}(\mathbf{b})\mathbf{a}. \quad (2)$$

If \mathbf{B} is a diagonal matrix, we have:

$$\text{vec}(\mathbf{ABC}) = (\mathbf{C}^T \diamond \mathbf{A})\text{vecd}(\mathbf{B}). \quad (3)$$

II. SYSTEM MODEL

Consider a narrowband single-user BD-RIS-assisted uplink MIMO system where the transmitter and receiver have M_T and M_R antennas, respectively, and the BD-RIS has N elements, as illustrated in Figure (1). The direct link between the transmitter and the receiver is assumed to be unavailable. We consider a group-connected BD-RIS architecture with Q groups comprising $\bar{N} = \frac{N}{Q}$ elements each, where the elements within each group are all connected. The received signal at the t -th symbol slot can be expressed as [11], [35]

$$\mathbf{y}_t = \sum_{q=1}^Q \mathbf{H}^{(q)} \mathbf{S}^{(q)} \mathbf{G}^{(q)} \mathbf{x}_t + \mathbf{z}_t^{(q)}, \quad (4)$$

where $\mathbf{H}^{(q)} \in \mathbb{C}^{M_R \times \bar{N}}$ and $\mathbf{G}^{(q)} \in \mathbb{C}^{\bar{N} \times M_T}$ represent the RIS-BS and UT-RIS channels, respectively, while $\mathbf{S}^{(q)} \in \mathbb{C}^{\bar{N} \times \bar{N}}$ denotes the (non-diagonal) scattering matrix associated with the q -th group. Additionally, $\mathbf{x}_t \in \mathbb{C}^{M_T \times 1}$ represents the data symbol vector, while $\mathbf{z}_t^{(q)}$ corresponds to the additive white Gaussian noise (AWGN) term.

The transmission protocol is illustrated in Figure 2. We consider a structured block transmission scheme, where the semi-blind channel estimation (CE) period consists of I frames, where each frame contains K data blocks of T symbol slots each, such that $T_c = KTI$. For each frame, the scattering matrix is assumed to change from block to block, while remaining unchanged during a block, i.e., the set of scattering matrices is repeated during all frames. We assume that the data symbols are encoded in each block using a Khatri-Rao coding scheme [19]. Moreover, to deal with some level of user mobility, the UT-RIS channel linking the user to the RIS is assumed to vary from frame to frame. In contrast, the RIS-BS channel remains unchanged during the whole transmission time. This assumption is reasonable since the BS and RIS are usually deployed at fixed positions, while the UT is a mobile node. Under these assumptions, the signal received during the t -th symbol slot of the k -th block and i -th frame can be expressed as

$$\mathbf{y}_{i,k,t} = \sum_{q=1}^Q \mathbf{H}^{(q)} \mathbf{S}_k^{(q)} \mathbf{G}_i^{(q)} \text{diag}(\mathbf{w}_k) \mathbf{x}_t + \mathbf{z}_{i,k,t}^{(q)}, \quad (5)$$

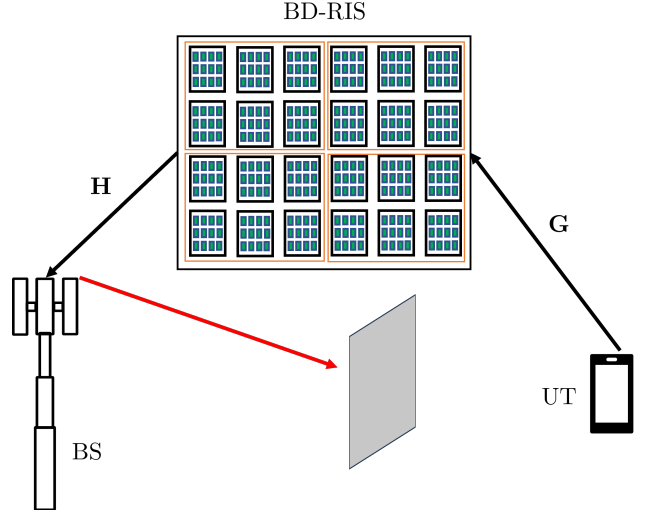


Fig. 1. Scenario of wireless communication assisted by BD-RIS.

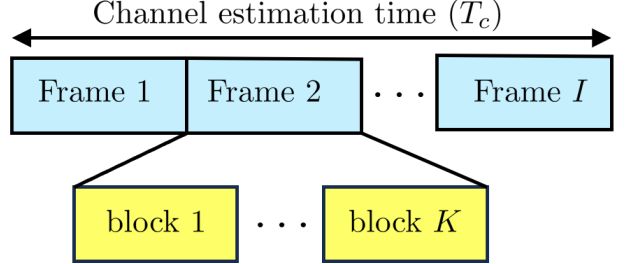


Fig. 2. Transmission protocol time structure: The channel estimation slot is divided into I frames each frame composed by K blocks.

where \mathbf{w}_k is the coding vector at the k -th block. Collecting the received signals during T time slots at a given frame i and block k , we get

$$\begin{aligned} \mathbf{Y}_{i,k} &= \sum_{q=1}^Q \mathbf{H}^{(q)} \mathbf{S}_k^{(q)} \mathbf{G}_i^{(q)} \text{diag}(\mathbf{w}_k) \mathbf{X}^T + \mathbf{Z}_{i,k} \\ &= \left(\sum_{q=1}^Q \mathbf{H}^{(q)} \mathbf{S}_k^{(q)} \mathbf{G}_i^{(q)} \right) \text{diag}(\mathbf{w}_k) \mathbf{X}^T + \mathbf{Z}_{i,k} \in \mathbb{C}^{M_r \times T}, \end{aligned} \quad (6)$$

where $\mathbf{X} = [\mathbf{x}_1, \dots, \mathbf{x}_T]^T \in \mathbb{C}^{T \times M_T}$ denotes the data symbol matrix, and $\mathbf{Z}_{i,k} \in \mathbb{C}^{M_r \times T}$ is the AWGN term³.

A. Scattering Matrix Design

The design of the BD-RIS scattering matrix used for training is fundamental to the uniqueness of the separate estimates of the involved communication channels. A baseline design for an LS channel estimation was first proposed in [11], [35], accounting for the physical constraints of the BD-RIS while ensuring energy conservation and the unitary property. Here, we consider an alternative scattering matrix design tailored to the proposed semi-blind channel and symbol estimation approach. Starting from the fundamental signal model in (6), we propose designing the BD-RIS matrix as

³From this point of the document we suppressed the noise term for simplicity. However, in the simulations, the noise is included.

the product of a fixed (static) scattering matrix \mathbf{S}_0 and a time-varying block-dependent diagonal rotation⁴, such that $\mathbf{S}_k^{(q)} = \mathbf{S}_0 \text{diag}(\bar{\mathbf{p}}_k^{(q)})$ where $\bar{\mathbf{p}}_k^{(q)}$ is the vector containing the phase rotation angles associated with the q -th group and the k -th block. Different from the state-of-the-art [11] and [18], the proposed design has a lower complex implementation since only the diagonal term $\bar{\mathbf{p}}_k^{(q)}$ changes per group. The proposed design also maintains the unitary property of the scattering matrix, as in [11], i.e.,

$$(\mathbf{S}_k^{(q)})^H \mathbf{S}_k^{(q)} = \mathbf{S}_k^{(q)} (\mathbf{S}_k^{(q)})^H = \mathbf{I}_{\bar{N}} \quad \forall q. \quad (7)$$

To meet this constraint, the static component \mathbf{S}_0 can be chosen as any unitary/orthogonal matrix (e.g., a truncated discrete Fourier transform (DFT) or Hadamard matrix). On the other hand, to ensure the identity in (7), the following condition must be satisfied:

$$\text{diag}(\bar{\mathbf{p}}_k^{(q)})^H \text{diag}(\bar{\mathbf{p}}_k^{(q)}) = \text{diag}(\bar{\mathbf{p}}_k^{(q)}) \text{diag}(\bar{\mathbf{p}}_k^{(q)})^H = \mathbf{I}_{\bar{N}} \quad \forall q. \quad (8)$$

Define $\bar{\mathbf{P}}^{(q)} = [\bar{\mathbf{p}}_1^{(q)}, \dots, \bar{\mathbf{p}}_K^{(q)}]^T \in \mathbb{C}^{K \times \bar{N}}$, the diagonal rotation component can be chosen to meet the following condition

$$(\bar{\mathbf{P}}^{(q)})^* \odot \bar{\mathbf{P}}^{(q)} = \bar{\mathbf{P}}^{(q)} \odot (\bar{\mathbf{P}}^{(q)})^* = \mathbf{1}_{K \times \bar{N}} \quad \forall q. \quad (9)$$

The design that satisfies (9) requires that

$$|\bar{\mathbf{P}}_{k\bar{n}}^{(q)}| = 1, \quad \forall k = 1, \dots, K \text{ and } \forall \bar{n} = 1, \dots, \bar{N}, \quad (10)$$

which means that the entries of the rotation matrix must belong to the complex unitary circle, for example, $\bar{\mathbf{P}}_{k\bar{n}}^{(q)} = e^{i\theta_{k\bar{n}}}$ with $\theta_{k\bar{n}} \in [0, 2\pi)$.

B. Received Signal Model

By considering the scattering matrix design discussed in Section II-A, the noiseless⁵ received signal given in (6) associated with frame i and block k can be expressed as

$$\mathbf{Y}_{i,k} = \left(\sum_{q=1}^Q \mathbf{H}^{(q)} \mathbf{S}_0^{(q)} \text{diag}(\bar{\mathbf{p}}_k^{(q)}) \mathbf{G}_i^{(q)} \right) \text{diag}(\mathbf{w}_k) \mathbf{X}^T, \quad (11)$$

which can be equivalently written as

$$\begin{aligned} \mathbf{Y}_{i,k} &= [\mathbf{H}^{(1)} \mathbf{S}_0^{(1)} \dots \mathbf{H}^{(Q)} \mathbf{S}_0^{(Q)}] \text{diag}(\mathbf{p}_k) \mathbf{G}_i \text{diag}(\mathbf{w}_k) \mathbf{X}^T \\ &= [\mathbf{H}^{(1)} \dots \mathbf{H}^{(Q)}] \mathbf{S} \text{diag}(\mathbf{p}_k) \mathbf{G}_i \text{diag}(\mathbf{w}_k) \mathbf{X}^T \\ &= \mathbf{H} \mathbf{S} \text{diag}(\mathbf{p}_k) \mathbf{G}_i \text{diag}(\mathbf{w}_k) \mathbf{X}^T \end{aligned} \quad (12)$$

⁴In contrast to the traditional BD-RIS modeling in [11], where the scattering matrix is constant, the work in [18] proposes varying the scattering matrix over time. However, this approach implies dynamically changing physical connections, which can be complex to implement. In our method, this factorization simplifies analysis and optimization by decoupling the immutable physical structure from the reconfigurable electronic controls. Specifically, \mathbf{S}_0 can represent the surface's static, inherent physical properties—such as inter-element coupling and mutual impedance, which define the complex wave-propagation pathways. In contrast, \mathbf{P} can represent the active control that applies individual phase shifts to dynamically steer the overall response (similar to the traditional RIS).

⁵We omit the noise term here for notation convenience. The noise contribution will be added later.

or, compactly,

$$\mathbf{Y}_{i,k} = \mathbf{H} \mathbf{S} \mathbf{D}_k(\mathbf{P}) \mathbf{G}_i \mathbf{D}_k(\mathbf{W}) \mathbf{X}^T, \quad (13)$$

where $\mathbf{G}_i = \left[(\mathbf{G}_i^{(1)})^T \dots (\mathbf{G}_i^{(Q)})^T \right]^T \in \mathbb{C}^{N \times M_T}$ and $\mathbf{H} = [\mathbf{H}^{(1)} \dots \mathbf{H}^{(Q)}] \in \mathbb{C}^{M_R \times N}$ are the two involved channel matrices collecting the contributions from all groups. Let us define $\mathbf{p}_k = [\mathbf{p}_k^{(1)T}, \dots, \mathbf{p}_k^{(Q)T}]^T \in \mathbb{C}^{N \times 1}$ and $\mathbf{S} \doteq \text{bdiag}(\mathbf{S}_0^{(1)}, \dots, \mathbf{S}_0^{(Q)}) \in \mathbb{C}^{N \times N}$, and note that $\mathbf{S} \mathbf{S}^H = \mathbf{I}_N$ since $\mathbf{S}_0^{(q)} \mathbf{S}_0^{(q)H} = \mathbf{I}_{\bar{N}}$. Additionally, define $\mathbf{P} = [\mathbf{p}_1, \dots, \mathbf{p}_K]^T \in \mathbb{C}^{K \times N}$, with $\mathbf{P}^H \odot \mathbf{P} = \mathbf{P} \odot \mathbf{P}^H = \mathbf{1}_N$ and $\mathbf{W} \doteq [\mathbf{w}_1, \dots, \mathbf{w}_K]^T \in \mathbb{C}^{K \times M_T}$ as the BD-RIS phase rotation matrix and transmit coding matrix, respectively.

The noiseless signal model in (13) corresponds to a PARATUCK-(2,4) decomposition of the fourth-order tensor $\mathbf{Y} \in \mathbb{C}^{M_R \times T \times K \times I}$, which belongs to the family of PARATUCK-type decompositions [36]. As a hybrid of the PARAFAC and TUCKER decompositions, it combines the uniqueness of the former with the flexibility of the latter.

Remark 1: Observe that, based on our proposed design for the BD-RIS scattering matrix, we can mask the dimension related to the number of blocks. This implies that, unlike other works in the literature [11], [18], our proposed method is more flexible, as the choice of system parameters depends only on well-known spatial and temporal domains, such as the number of antennas and time slots. This will become clearer in the identifiability condition section (Section IV).

III. SEMI-BLIND RECEIVERS

We propose a data-driven approach to provide separate estimates of the involved channel matrices without the need of pilot sequences. This can be achieved by exploiting a tensor algebraic signal structure according to a PARATUCK-(2,4) decomposition of the received signal in (13). We formulate two semi-blind receivers that exploit the intrinsic algebraic structure of the received signal tensor in two different ways. The common feature of both receivers is to leverage useful data symbols to achieve decoupled estimates of the two channel matrices. The tradeoffs between the two receiver algorithms in terms of performance, complexity, and operating conditions are also discussed.

A. PARAFAC-Based Receiver

The received signal model in (13) involves three unknown system matrices, namely, the static channel matrix \mathbf{H} linking the BD-RIS and the BS, the block-dependent channel matrix \mathbf{G}_i linking the UT and BD-RIS, and the symbol matrix \mathbf{X} .

Note that the vectorized version of the received signal in frame- i block- k is

$$\mathbf{y}_{i,k} = \text{vec}(\mathbf{Y}_{i,k}) = (\mathbf{X} \otimes \mathbf{H} \mathbf{S}) (\mathbf{D}_k(\mathbf{W}) \otimes \mathbf{D}_k(\mathbf{P})) \mathbf{g}_i, \quad (14)$$

such that applying the property (2) in (14), we have

$$\text{vec}(\mathbf{Y}_{i,k}) = (\mathbf{X} \otimes \mathbf{H} \mathbf{S}) \text{diag}(\mathbf{g}_i) (\mathbf{W}_{k\cdot}^T \otimes \mathbf{P}_{k\cdot}^T). \quad (15)$$

Then, collecting the signal from all of the K data blocks $\mathbf{Y}_i = [\text{vec}(\mathbf{Y}_{i,1}) \text{ vec}(\mathbf{Y}_{i,2}) \dots \text{ vec}(\mathbf{Y}_{i,K})]$, we have the received signal at frame i as

$$\begin{aligned}\mathbf{Y}_i &= [\mathbf{y}_{i,1} \mathbf{y}_{i,2} \dots \mathbf{y}_{i,K}] \\ &= (\mathbf{X} \otimes \mathbf{H}\mathbf{S}) \text{diag}(\mathbf{g}_i) [\mathbf{W}_{1.}^T \otimes \mathbf{P}_{1.}^T \dots \mathbf{W}_{K.}^T \otimes \mathbf{P}_{K.}^T] \\ &= (\mathbf{X} \otimes \mathbf{H}\mathbf{S}) \text{diag}(\mathbf{g}_i) (\mathbf{W}^T \diamond \mathbf{P}^T) \in \mathbb{C}^{M_R T \times K}.\end{aligned}\quad (16)$$

Indeed, (16), is a 3-mode unfolding transposed $[\mathbf{Y}_i]_{(3)}^T$ of the tensor $\mathbf{Y}_i \in \mathbb{C}^{M_R \times T \times K}$ that fits a third-order TUCKER tensor model whose the n -mode product is given as

$$\mathbf{Y}_i = \mathcal{T}_{\mathbf{G}_i} \times_1 \mathbf{H}\mathbf{S} \times_2 \mathbf{X} \times_3 (\mathbf{W}^T \diamond \mathbf{P}^T)^T, \quad (17)$$

where the 3-mode unfolding of the tensor $[\mathcal{T}_{\mathbf{G}_i}]_{(3)}$ coincides with $\text{diag}(\mathbf{g}_i)$, that is, $[\mathcal{T}_{\mathbf{G}_i}]_{(3)} = \text{diag}(\mathbf{g}_i)$. Defining

$$\Omega \doteq (\mathbf{X} \otimes \mathbf{H}\mathbf{S}) \in \mathbb{C}^{T M_R \times M_T N}, \quad (18)$$

and

$$\Psi^T \doteq (\mathbf{W}^T \diamond \mathbf{P}^T) \in \mathbb{C}^{M_T N \times K}, \quad (19)$$

we have

$$[\mathbf{Y}_i]_{(3)}^T = \Omega [\mathcal{T}_{\mathbf{G}_i}]_{(3)} \Psi^T \in \mathbb{C}^{T M_R \times K}. \quad (20)$$

Let $\mathbf{Z} \in \mathbb{C}^{T M_R \times K \times I}$ be a third order tensor which is defined as

$$\mathbf{Z} \doteq [\mathbf{Y}_1]_{(3)}^T \sqcup_3 [\mathbf{Y}_2]_{(3)}^T \dots \sqcup_3 [\mathbf{Y}_I]_{(3)}^T, \quad (21)$$

such that

$$\mathbf{Z} = \mathcal{I}_{3, M_T N} \times_1 \Omega \times_2 \Psi \times_3 \bar{\mathbf{G}}, \quad (22)$$

where $\bar{\mathbf{G}} = [\mathbf{g}_1 \dots \mathbf{g}_I]^T \in \mathbb{C}^{I \times M_T N}$. Note that \mathbf{Z} matches a third-order PARAFAC tensor model [37]. In Figure 2, we illustrate the procedures run until this point. It can be noted that the received signal model $\mathbf{Y}_{i,k}$ is a PARATUCK(2,4), which is a fourth-order tensor \mathbf{Y} . Concatenating this tensor via the vectorized version related to the 3-mode K , for each frame we have a third-order tensor $\mathbf{Y}_i \in \mathbb{C}^{M_R \times T \times K}$ that matches a third-order TUCKER model, $i = 1, \dots, I$. However, the 3-mode unfolding transposed of \mathbf{Y}_i can be seen as the i -th frontal slice of a tensor $\mathbf{Z} \in \mathbb{C}^{M_R T \times K \times I}$ that fits a PARAFAC model where the factor matrices are structured. Let us recall that Ω is the Kronecker product between the data symbols \mathbf{X} and the equivalent channel $\mathbf{H}\mathbf{S}$ while Ψ is the Khatri-Rao (column-wise Kronecker) product between the rotation matrix \mathbf{P} and the coding matrix \mathbf{W} . In this sense, the following correspondence can be established:

$$\begin{aligned}(\mathbf{A}, \mathbf{B}, \mathbf{C}) &\leftrightarrow (\Omega, \Psi, \bar{\mathbf{G}}) \\ (I_1, I_2, I_3) &\leftrightarrow (T M_R, K, I).\end{aligned}\quad (23)$$

To estimate the factor matrix Ω and the channel $\bar{\mathbf{G}}$, we must solve the following optimization problem

$$(\hat{\bar{\mathbf{G}}}, \hat{\Omega}) = \arg \min_{\bar{\mathbf{G}}, \Omega} \|\mathbf{Z} - \mathcal{I}_{3, M_T N} \times_1 \Omega \times_2 \Psi \times_3 \bar{\mathbf{G}}\|_F^2, \quad (24)$$

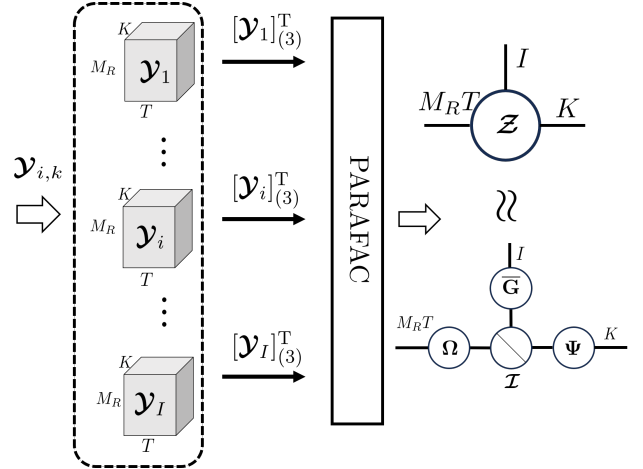


Fig. 3. Third-order PARAFAC tensor model: The received signal at (14) fits a fourth-order PARATUCK tensor model. From the third mode unfolding of the tensor $\mathbf{Y}_{i,k}$, we derive a third-order PARAFAC model, with Ω , Ψ and $\bar{\mathbf{G}}$ as factor matrices.

Note that (24) is a nonlinear problem due to the presence of two unknown matrices $(\bar{\mathbf{G}}$ and Ω). To address this issue, we can derive sub-optimization linear programs that hold certain matrices constant. For instance, by fixing the channel matrix $\bar{\mathbf{G}}$, the problem becomes linear in the factor matrix Ω . Similarly, fixing Ω we have a linear problem in $\bar{\mathbf{G}}$. Consequently, the optimization problem in (24) can be decomposed into sub-optimization problems, which can then be solved iteratively. This is the underlying premise of the alternating least squares (ALS) algorithm. On the other hand, since we are interested in solving only for Ω and $\bar{\mathbf{G}}$, the algorithm is defined as bilinear alternating least squares (BALS). For this, we shall make use of $[\mathbf{Z}]_{(1)}$ and $[\mathbf{Z}]_{(3)}$, which from (20), are defined as

$$\begin{aligned}[\mathbf{Z}]_{(1)} &= [[\mathbf{Y}_1]_{(3)}^T [\mathbf{Y}_2]_{(3)}^T \dots [\mathbf{Y}_I]_{(3)}^T] \\ &= \Omega [\text{diag}(\mathbf{g}_1) \Psi^T \text{diag}(\mathbf{g}_2) \Psi^T \dots \text{diag}(\mathbf{g}_I) \Psi^T] \\ &= \Omega (\bar{\mathbf{G}} \diamond \Psi)^T \in \mathbb{C}^{T M_R \times I K},\end{aligned}\quad (25)$$

and

$$\begin{aligned}[\mathbf{Z}]_{(3)} &= [\text{vec}([\mathbf{Y}_1]_{(3)}^T) \text{ vec}([\mathbf{Y}_2]_{(3)}^T) \dots \text{ vec}([\mathbf{Y}_I]_{(3)}^T)]^T \\ &= [(\Psi \diamond \Omega) [\mathbf{g}_1 \mathbf{g}_2 \dots \mathbf{g}_I]]^T \\ &= \bar{\mathbf{G}} (\Psi \diamond \Omega)^T \in \mathbb{C}^{I \times K T M_R}.\end{aligned}\quad (26)$$

By exploiting the first and third mode unfoldings, as described in equations (25) and (26), respectively, we propose an iterative solution to estimate the structured matrix Ω and the channel matrix $\bar{\mathbf{G}}$. It is important to note that after estimating Ω , a Kronecker factorization problem must be solved to recover the data symbol matrix \mathbf{X} and the BS-IRS channel \mathbf{H} . This results in a two-stage solution: first, we solve the PARAFAC problems using the BALS algorithm, followed by a Kronecker factorization problem. Due to this combined approach, we have titled this algorithm PAKRON (Algorithm 1).

Algorithm 1: PAKRON receiver

Procedure
input : Received signal \mathcal{Z}
output: $\hat{\mathbf{X}}$, $\hat{\mathbf{H}}$ and $\hat{\mathbf{G}}$

begin

- 1. Run stage I using Algorithm 2
- 2. Run stage II using Algorithm 3

end

Algorithm 2: Stage I of the PAKRON receiver

Procedure
input : Received signal \mathcal{Z}
output: $\hat{\Omega}$, $\hat{\mathbf{G}}$

to $i = 0$ initialize $\hat{\mathbf{G}}_{(i=0)}$ **begin**

- $i = i + 1$;
- while** $\|e(i) - e(i-1)\| \geq \delta$ **do**

 - 1: Find a least squares estimate of $\hat{\Omega}_i$:
 $\hat{\Omega}_i = [\mathcal{Y}]_{(1)} [(\hat{\mathbf{G}}_{(i-1)} \diamond \Psi)^T]^\dagger$
 - 2: Find a least squares estimate of $\hat{\mathbf{G}}_i$:
 $\hat{\mathbf{G}}_i = [\mathcal{Y}]_{(3)} [(\Psi \diamond \hat{\Omega}_i)^T]^\dagger$
 - 3: Repeat steps 1 to 2 until convergence.

- end**

end

1) *PAKRON receiver (Stage I):* By exploiting the matrix unfoldings (25) and (26), we derive the BALS algorithm. This algorithm estimates the matrices Ω and $\bar{\mathbf{G}}$ in an alternating manner by iteratively optimizing the following two cost functions:

$$\hat{\Omega} = \arg \min_{\bar{\mathbf{G}}} \left\| [\mathcal{Y}]_{(1)} - \Omega (\bar{\mathbf{G}} \diamond \Psi)^T \right\|_F^2, \quad (27)$$

$$\hat{\mathbf{G}}^T = \arg \min_{\Omega} \left\| [\mathcal{Y}]_{(3)} - \bar{\mathbf{G}}^T (\Psi \diamond \Omega)^T \right\|_F^2, \quad (28)$$

the solutions of which are respectively given by

$$\hat{\Omega} = [\mathcal{Y}]_{(1)} \left[(\bar{\mathbf{G}} \diamond \Psi)^T \right]^\dagger, \quad (29)$$

$$\hat{\mathbf{G}} = [\mathcal{Y}]_{(3)} \left[(\Psi \diamond \Omega)^T \right]^\dagger. \quad (30)$$

The convergence of Algorithm 4 is declared when $\|e_{(i)} - e_{(i-1)}\| \leq \delta$, where $e_{(i)} = \|\mathcal{Y} - \hat{\mathcal{Y}}_{(i)}\|_F^2$ denotes the reconstruction error computed at the i -th iteration. δ is a predefined threshold parameter, and $\hat{\mathcal{Y}}_{(i)} = [\hat{\mathbf{G}}_{(i)}, \hat{\Omega}_{(i)}, \Psi]$ is the reconstructed PARAFAC model at the i -th iteration. From Stage I, we obtain an estimate of Ω , as defined in equation (18), which is subsequently used in Stage II.

2) *PAKRON receiver (Stage II):* In Stage II, the estimation of the data symbol matrix \mathbf{X} and the RIS-BS channel \mathbf{H} is achieved by solving the following optimization problem:

$$(\hat{\mathbf{X}}, \hat{\mathbf{H}}) = \arg \min_{\mathbf{X}, \mathbf{H}} \|\Delta - \mathbf{X} \otimes \mathbf{H}\|_F^2. \quad (31)$$

Algorithm 3: Stage II of the PAKRON receiver

Procedure
input : $\hat{\Omega}$
output: $\hat{\mathbf{X}}$ and $\hat{\mathbf{H}}$

begin

- 1. Construct the rank-one matrix $\tilde{\Delta} \in \mathbb{C}^{TM_T \times M_R N}$
- 2. $(\mathbf{u}_1, \sigma_1, \mathbf{v}_1) \leftarrow$ truncated-SVD($\tilde{\Delta}$)
- $\hat{\mathbf{x}} \leftarrow \sqrt{\sigma_1} \mathbf{u}_1$; $\hat{\mathbf{h}} \leftarrow \sqrt{\sigma_1} \mathbf{v}_1^*$
- 3. Reconstruct $\hat{\mathbf{X}}$ and $\hat{\mathbf{H}}$ by unvec $\hat{\mathbf{x}}$ and $\hat{\mathbf{h}}$
- 4. Remove the scaling ambiguities of $\hat{\mathbf{X}}$ and $\hat{\mathbf{H}}$.

end

where $\Delta = \hat{\Omega} (\mathbf{I}_{M_T} \otimes \mathbf{S}^H)$. The matrix $\bar{\mathbf{Z}}$ can be approximated as a rank one matrix Δ , such that:

$$\tilde{\Delta} = \begin{bmatrix} x_{1,1} \text{vec}(\mathbf{H}) & \dots & x_{T,UL} \text{vec}(\mathbf{H}) \end{bmatrix}^T = \text{vec}(\mathbf{X}) \text{vec}(\mathbf{H})^T \in \mathbb{C}^{TM_T \times M_R N}. \quad (32)$$

This implies that solving the problem in (31) is equivalent to solving the following problem:

$$(\hat{\mathbf{X}}, \hat{\mathbf{H}}) = \min_{\mathbf{X}, \mathbf{H}} \|\tilde{\mathbf{Z}} - \mathbf{x} \mathbf{h}^T\|_F, \quad (33)$$

where $\mathbf{x} = \text{vec}(\mathbf{X})$ and $\mathbf{h} = \text{vec}(\mathbf{H})$. According to [38], the optimal solution for estimating the vectorized version of the RIS-BS channel and the data symbol matrix is obtained by taking the left and right singular vectors of $\tilde{\Delta}$, as illustrated in Algorithm 3.

B. TUCKER-Based Receiver

The approach developed in Section III-A combines the temporal domain (number of time slots, T) with the spatial domain (number of receiver antennas, M_R), yielding a structured PARAFAC model. As a consequence, a two-stage joint symbol and channel estimation is performed, which may lead to error propagation and degrade system performance in noise-limited scenarios. However, alternative strategies can be applied to rearrange the received signal, as illustrated in Figure 4, where two temporal dimensions (frames I and blocks K) are combined. Then, let us revisit the received signal at (16)

$$\mathbf{Y}_i = (\mathbf{X} \otimes \mathbf{H} \mathbf{S}) \text{diag}(\mathbf{g}_i) \Psi^T, \quad (34)$$

and its 1-mode unfolding in (25)

$$\begin{aligned} [\mathcal{Y}]_{(1)} &= [\mathbf{Y}_1 \ \mathbf{Y}_2 \ \dots \ \mathbf{Y}_I] \\ &= (\mathbf{X} \otimes \mathbf{H} \mathbf{S}) (\bar{\mathbf{G}} \diamond \Psi)^T \in \mathbb{C}^{TM_R \times IK}. \end{aligned} \quad (35)$$

Note that the equation (35) can be seen as a third order tensor $\tilde{\mathcal{Y}} \in \mathbb{C}^{M_R \times T \times IK}$ that corresponds to a TUCKER model where the its n -mode product is

$$\tilde{\mathcal{Y}} = (\bar{\mathbf{G}} \diamond_3 \mathcal{T}) \times_1 \mathbf{H} \mathbf{S} \times_2 \mathbf{X} \times_3 \mathbf{I}_{IK} \in \mathbb{C}^{M_R \times T \times IK}, \quad (36)$$

where the core tensor $\mathcal{C} = (\bar{\mathbf{G}} \diamond_3 \mathcal{T}) \in \mathbb{C}^{N \times M_T \times IK}$ has a special structure which is given by 3-mode Khatri-Rao product between two tensors, which are

$$\bar{\mathbf{G}} \doteq [\bar{\mathbf{G}}_1 \sqcup_3 \bar{\mathbf{G}}_2 \sqcup_3 \dots \sqcup_3 \bar{\mathbf{G}}_I] \in \mathbb{C}^{N \times M_T \times I} \quad (37)$$

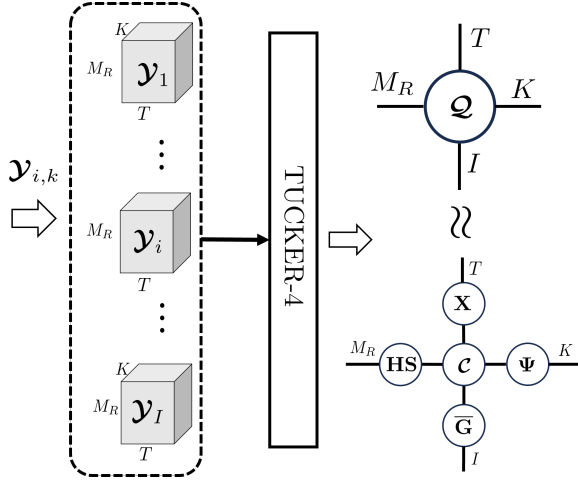


Fig. 4. TUCKER tensor model: In this scenario, the tensor from i -th frame, \mathbf{Y}_i in (18), is rearranged to derive a fourth-order TUCKER model for the received signal tensor.

and

$$\mathcal{T} \doteq \mathcal{I}_{3,K} \times_1 \mathbf{P}^T \times_2 \mathbf{W}^T \times_3 \mathbf{I}_K \in \mathbb{C}^{N \times M_T \times K}. \quad (38)$$

Note that the channel $\bar{\mathbf{G}}$ lies within the core tensor. This implies that, in a straightforward approach, one would need at least a two-stage procedure: first estimate the core tensor, then extract $\bar{\mathbf{G}}$. Instead of reducing the tensor order, however, we can preserve the fourth-order structure and reinterpret it as a TUCKER model. This can be done by applying the multimode unfolding concept, which reveals that the PARATUCK-(2,4) model can be expressed as a fourth-order TUCKER tensor model. This relationship is depicted in Fig. 4, where the I tensors \mathbf{Y}_i ($i = 1, \dots, I$) are transformed, via multimode unfolding, into a TUCKER tensor \mathbf{Q} (in tensor network notation). This transformation preserves the original dimensions but changes the underlying tensor model. Such a reformulation enables the derivation of a single-stage solution, as discussed next.

We know that given $\mathbf{A} \in \mathbb{C}^{N_A \times L}$ and $\mathbf{B} \in \mathbb{C}^{N_B \times L}$, the Khatri-Rao product between them can be expressed as $\mathbf{A} \diamond \mathbf{B} = (\mathbf{A} \otimes \mathbf{B}) \Xi \in \mathbb{C}^{N_A N_B \times L}$ where Ξ is an $L^2 \times L$ selection matrix that extracts the column-wise Kronecker product. Now, applying this Khatri-Rao and Kronecker product relationship to the 1-mode unfolding in (35), we can rewrite it as

$$\begin{aligned} [\mathbf{Y}]_{(1)} &= (\mathbf{X} \otimes \mathbf{H} \mathbf{S}) (\bar{\mathbf{G}} \diamond \Psi)^T \in \mathbb{C}^{T M_R \times I K} \\ &= (\mathbf{X} \otimes \mathbf{H} \mathbf{S}) ((\bar{\mathbf{G}} \otimes \Psi) \Xi)^T \\ &= (\mathbf{X} \otimes \mathbf{H} \mathbf{S}) \Xi^T (\bar{\mathbf{G}} \otimes \Psi)^T, \end{aligned} \quad (39)$$

where $\Xi \in \mathbb{C}^{(M_T N)^2 \times M_T N}$ is the selection matrix such that $\Xi = \mathbf{I}_{M_T N} \diamond \mathbf{I}_{M_T N}$. From these observations, we can note that $[\mathbf{Y}]_{(1)}$ can be seen as a generalized unfolding of a tensor \mathbf{Q} , this is $[\mathbf{Q}]_{([1,2],[3,4])} = [\mathbf{Y}]_{(1)}$. Then,

$$[\mathbf{Q}]_{([1,2],[3,4])} = (\mathbf{X} \otimes \mathbf{H} \mathbf{S}) (\mathbf{I}_{M_T N} \diamond \mathbf{I}_{M_T N})^T (\bar{\mathbf{G}} \otimes \Psi)^T, \quad (40)$$

where $(\mathbf{I}_{M_T N} \diamond \mathbf{I}_{M_T N})^T = [\mathbf{C}]_{([1,2],[3,4])} \in \mathbb{C}^{M_T N \times (M_T N)^2}$ is the multimode unfolding of a fourth-order core tensor $\mathbf{C} \in \mathbb{C}^{N \times M_T \times M_T N \times M_T N}$ while the equation (40) denotes the multimode unfolding of the tensor $\mathbf{Q} \in \mathbb{C}^{M_R \times T \times K \times I}$, whose the n -mode product notation is

$$\mathbf{Q} = \mathbf{C} \times_1 \mathbf{H} \mathbf{S} \times_2 \mathbf{X} \times_3 \Psi \times_4 \bar{\mathbf{G}}. \quad (41)$$

The fourth-order tensor \mathbf{Q} fits a TUCKER model, where the matrix Ψ is known. To estimate the matrices $\mathbf{H} \mathbf{S}$, \mathbf{X} and $\bar{\mathbf{G}}$ it is necessary to solve the following optimization problem:

$$\arg \min_{(\mathbf{H} \mathbf{S}, \mathbf{X}, \bar{\mathbf{G}})} \|\mathbf{Q} - \mathbf{C} \times_1 \mathbf{H} \mathbf{S} \times_2 \mathbf{X} \times_3 \Psi \times_4 \bar{\mathbf{G}}\|_F^2. \quad (42)$$

The problem in (42) is nonlinear since the three factor matrices are unknown. However, it can be unfolded into a fourth-order model formulation in terms of its factor matrices as follows:

$$[\mathbf{Q}]_{(1)} = \mathbf{H} \mathbf{S} [\mathbf{C}]_{(1)} (\bar{\mathbf{G}} \otimes \Psi \otimes \mathbf{X})^T \in \mathbb{C}^{M_R \times I K T}, \quad (43)$$

$$[\mathbf{Q}]_{(2)} = \mathbf{X} [\mathbf{C}]_{(2)} (\bar{\mathbf{G}} \otimes \Psi \otimes \mathbf{H} \mathbf{S})^T \in \mathbb{C}^{T \times I K M_R}, \quad (44)$$

$$[\mathbf{Q}]_{(3)} = \Psi [\mathbf{C}]_{(3)} (\bar{\mathbf{G}} \otimes \mathbf{X} \otimes \mathbf{H} \mathbf{S})^T \in \mathbb{C}^{K \times I T M_R}, \quad (45)$$

$$[\mathbf{Q}]_{(4)} = \bar{\mathbf{G}} [\mathbf{C}]_{(4)} (\Psi \otimes \mathbf{X} \otimes \mathbf{H} \mathbf{S})^T \in \mathbb{C}^{I \times K T M_R}, \quad (46)$$

with $[\mathbf{C}]_{(1)} \in \mathbb{C}^{N \times (M_T N)^2 M_T}$, $[\mathbf{C}]_{(2)} \in \mathbb{C}^{M_T \times (M_T N)^2 N}$, $[\mathbf{C}]_{(3)} \in \mathbb{C}^{M_T N \times (M_T N)^2}$ and $[\mathbf{C}]_{(4)} \in \mathbb{C}^{M_T N \times (M_T N)^2}$. From the first, second, and fourth mode unfoldings, we can derive three sub-optimization linear problems as given

$$\arg \min_{(\mathbf{H} \mathbf{S})} \|[\mathbf{Q}]_{(1)} - \mathbf{H} \mathbf{S} [\mathbf{C}]_{(1)} (\bar{\mathbf{G}} \otimes \Psi \otimes \mathbf{X})^T\|_F^2, \quad (47)$$

$$\arg \min_{(\mathbf{X})} \|[\mathbf{Q}]_{(2)} - \mathbf{X} [\mathbf{C}]_{(2)} (\bar{\mathbf{G}} \otimes \Psi \otimes \mathbf{H} \mathbf{S})^T\|_F^2, \quad (48)$$

$$\arg \min_{(\bar{\mathbf{G}})} \|[\mathbf{Q}]_{(4)} - \bar{\mathbf{G}} [\mathbf{C}]_{(4)} (\Psi \otimes \mathbf{X} \otimes \mathbf{H} \mathbf{S})^T\|_F^2. \quad (49)$$

To estimate $\mathbf{H} \mathbf{S}$, \mathbf{X} and $\bar{\mathbf{G}}$, we solve alternately the LS problems in (47), (48) and (49), respectively, whose the solutions are given by:

$$\hat{\mathbf{H}} \mathbf{S} = [\mathbf{Q}]_{(1)} \left[[\mathbf{C}]_{(1)} (\bar{\mathbf{G}} \otimes \Psi \otimes \mathbf{X})^T \right]^\dagger \quad (50)$$

$$\hat{\mathbf{X}} = [\mathbf{Q}]_{(2)} \left[[\mathbf{C}]_{(2)} (\bar{\mathbf{G}} \otimes \Psi \otimes \mathbf{H} \mathbf{S})^T \right]^\dagger \quad (51)$$

$$\hat{\bar{\mathbf{G}}} = [\mathbf{Q}]_{(4)} \left[[\mathbf{C}]_{(4)} (\Psi \otimes \mathbf{X} \otimes \mathbf{H} \mathbf{S})^T \right]^\dagger. \quad (52)$$

This procedure is the foundation of the Trilinear Alternate Least Squares TUCKER receiver described in the Algorithm 4. The convergence criterion is similar to Algorithm 2. Note that this approach avoids the error propagation of the two-stage PAKRON solution.

Remark 2: From (45), an alternative (closed-form) approach can be used to jointly estimate the involved channels \mathbf{H} , \mathbf{G} as well as the data symbol matrix \mathbf{X} . This approach left-filters the 3-mode unfolding of the received signal using $(\Psi [\mathbf{C}]_{(1)})^\dagger$ followed by solving a “triple-Kronecker” factorization problem on the filtered signal. The algorithm is similar to the one proposed in [39]. Despite being a less complex estimation method, this approach imposes a more restrictive restriction on the data block length, requiring $K \geq (M_T N)^2$.

Algorithm 4: TUCKER receiver

Procedure
input : Received signal \mathbf{Q}
output: $\hat{\mathbf{H}}$, $\hat{\mathbf{G}}$ and $\hat{\mathbf{X}}$

```

to  $i = 0$  initialize  $\hat{\mathbf{G}}_{(i=0)}$  and  $\hat{\mathbf{X}}_{(i=0)}$  begin
   $i = i + 1$ ;
  while  $\|e(i) - e(i - 1)\| \geq \delta$  do
    1: Find a least squares estimate of  $\hat{\mathbf{H}}\mathbf{S}_i$ :
    
$$(\hat{\mathbf{H}}\mathbf{S})_i = [\mathbf{Q}]_{(1)} \left[ \underbrace{[\mathcal{C}]_{(1)} (\bar{\mathbf{G}}_{(i-1)} \otimes \mathbf{\Psi} \otimes \mathbf{X}_{(i-1)})^T}_{N \times IKT} \right]$$

    2: Find a least squares estimate of  $\hat{\mathbf{X}}_i$ :
    
$$\hat{\mathbf{X}}_i = [\mathbf{Q}]_{(2)} \left[ \underbrace{[\mathcal{C}]_{(2)} (\bar{\mathbf{G}}_{(i-1)} \otimes \mathbf{\Psi} \otimes (\mathbf{H}\mathbf{S})_i)^T}_{M_T \times IKT M_R} \right]^\dagger$$

    3: Find a least squares estimate of  $\hat{\mathbf{G}}_i$ :
    
$$\hat{\mathbf{G}}_i = [\mathbf{Q}]_{(4)} \left[ \underbrace{[\mathcal{C}]_{(4)} (\mathbf{\Psi} \otimes \mathbf{X}_i \otimes (\mathbf{H}\mathbf{S})_i)^T}_{M_T N \times KTM_R} \right]^\dagger$$

    4: Repeat steps 1 to 3 until convergence.
  end
end

```

IV. IDENTIFIABILITY AND COMPLEXITY

In this section, we discuss the identifiability conditions for our proposed solutions. The study provides a useful relationship among the system parameters necessary to obtain unique estimates of the channel matrices and the symbol matrix when using the proposed semi-blind receivers.

1) *TALS-TUCKER receiver*: For the TALS-TUCKER receiver, the problems (47), (48), and (49) are unique in the LS sense if $\mathbf{V}_1 = [\mathcal{C}]_{(1)} (\bar{\mathbf{G}} \otimes \mathbf{\Psi} \otimes \mathbf{X})^T \in \mathbb{C}^{N \times IKT}$, $\mathbf{V}_2 = [\mathcal{C}]_{(2)} (\bar{\mathbf{G}} \otimes \mathbf{\Psi} \otimes \mathbf{H}\mathbf{S})^T \in \mathbb{C}^{M_T \times IKT M_R}$ and $\mathbf{V}_4 = [\mathcal{C}]_{(4)} (\mathbf{\Psi} \otimes \mathbf{X} \otimes \mathbf{H}\mathbf{S})^T \in \mathbb{C}^{M_T N \times KTM_R}$ are full row rank. Satisfying these conditions implies the following inequalities

$$IKT \geq N, \quad IKT M_R \geq M_T \text{ and } KTM_R \geq M_T N. \quad (53)$$

Combining them, we obtain a necessary condition for the uniqueness of the TALS-TUCKER receiver in the LS sense, in terms of the required number of blocks as

$$K \geq \max \left(\frac{N}{IT}, \frac{M_T}{IM_R}, \frac{M_T N}{TM_R} \right). \quad (54)$$

2) *PAKRON receiver*: The conditions necessary to ensure a unique joint channel and symbol recovery for the PAKRON receiver are associated with stage I. In this sense, the problems (27) and (28) are unique in the LS sense if $\mathbf{R}_1 = \bar{\mathbf{G}} \diamond \mathbf{\Psi} \in \mathbb{C}^{IK \times M_T N}$ and $\mathbf{R}_2 = \mathbf{\Psi} \diamond \mathbf{\Omega} \in \mathbb{C}^{KTM_R \times M_T N}$ are full column rank, which implies the following conditions to be satisfied:

$$IK \geq M_T N \quad \text{and} \quad KTM_R \geq M_T N, \quad (55)$$

or, equivalently,

$$K \geq \frac{M_T N}{I} \quad \text{and} \quad K \geq \frac{M_T N}{TM_R} \quad (56)$$

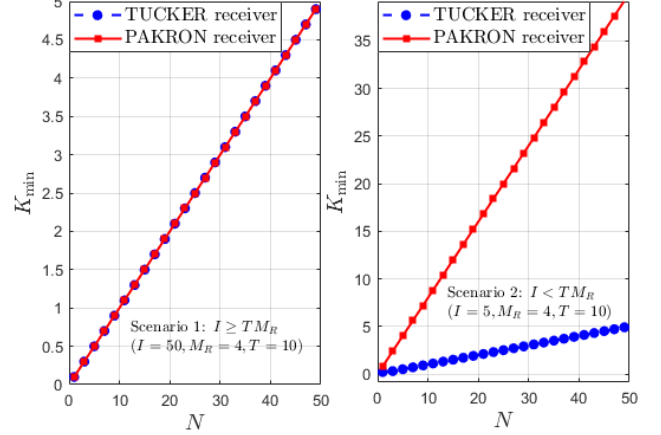


Fig. 5. Minimum number K of data blocks required for joint channel and symbol estimation for TUCKER and PAKRON semi-blind receivers, considering different BD-RIS sizes.

leading to the following bound on the required number of blocks

$$K \geq \max \left(\frac{M_T N}{I}, \frac{M_T N}{TM_R} \right). \quad (57)$$

It is important to note that inequalities (54) and (57) are easy-to-check necessary conditions for ensuring uniqueness of the joint channel and symbol matrix estimation. Additionally, they allow us to assess the degree of restriction imposed by the proposed solutions, thereby guiding the selection of appropriate system parameters for each semi-blind receiver, while shedding light on the trade-offs between both solutions. To verify the design constraints of the proposed solutions, we set M_T , M_R , and T constant and determined K_{\min} for two different scenarios as a function of N . Figure 5 illustrates that, in the first scenario, where $I \geq TM_R$, both receivers have the same K_{\min} . In contrast, in the second scenario, when $I < TM_R$, the TUCKER receiver is considerably less restrictive compared to the PAKRON method.

Additionally, the stage I of the PAKRON receiver enables the derivation of a sufficient uniqueness condition. Since \mathcal{Z} follows a third-order PARAFAC model, uniqueness is ensured if the so-called Kruskal condition is satisfied [40]

$$Kr(\mathbf{\Omega}) + Kr(\mathbf{\Psi}) + Kr(\bar{\mathbf{G}}) \geq 2M_T N + 2. \quad (58)$$

However, the received signal tensor exploited by the PAKRON receiver involves structured matrices. More specifically, in the PARAFAC decomposition (22), the first and second mode factor matrices have Kronecker and Khatri-Rao product structures, respectively, as shown in (18) and (19). Therefore, it is important to analyze how these structures influence the uniqueness condition (58). To this end, note that $\text{rank}(\mathbf{\Omega}) = \text{rank}(\mathbf{X} \otimes \mathbf{H}\mathbf{S}) = \text{rank}(\mathbf{X})\text{rank}(\mathbf{H}\mathbf{S})$. Considering $T \geq M_T$, and using the fact the $\mathbf{S} \in \mathbb{C}^{N \times N}$ is full rank by construction, we have

$$\text{rank}(\mathbf{\Omega}) = \text{Trank}(\mathbf{H}) = T \min(M_R, N). \quad (59)$$

Resorting to the lemma on the rank of the Khatri-Rao product (see [41]–[43]), and using the fact that \mathbf{W} and \mathbf{P}

are full-rank matrices by construction, Ψ has full-rank equal to K . Additionally, assuming scattering-rich propagation the Kruskal-rank condition (58) can be rewritten as a function of the system parameters as follows

$$K + T \min(M_R, N) + \min(I, M_T N) \geq 2M_T N + 2. \quad (60)$$

This condition sheds light on the balance of the system parameters to establish a sufficient condition for the PAKRON receiver to jointly estimate the channel and symbols uniquely.

Remark 3: It should be noted from (60) that various scenarios can be explored based on different system parameter configurations. In this context, it is also worth noting that the PAKRON receiver still operates in a more challenging scenario under rank-deficient channel models, as it may not satisfy condition (60). For instance, in the extreme case where the rank of the RIS-BS channel \mathbf{H} is one (which arises under line of sight (LoS) propagation between the BS and the RIS), we have from (59) that $\text{rank}(\Omega) = T$. In this case, when we collect a sufficient number of frames so that $I \geq M_T N$, condition (60) is automatically fulfilled. Otherwise, if $I < M_T N$, it becomes necessary to have $T + K + I \geq 2M_T N + 2$ in order to compensate for the rank deficiency of the channels.

Complexity: In algorithms involving pseudo-inverse calculations or rank-1 approximations, the computational complexity is generally dominated by the Singular Value Decomposition (SVD) [44]. Note that, for an arbitrary matrix $\mathbf{A} \in \mathbb{C}^{M \times N}$, the complexity of its SVD computation is $\mathcal{O}(MN \min(M, N))$. It can be noted that the complexity of solving an LS problem is dominated by the associated SVD computations. Considering that the PAKRON algorithm comprises two stages, we have: In Stage I, the computational complexity is primarily determined by steps 1 and 2, which have complexities of $\mathcal{O}((M_T N)^2 I K)$ and $\mathcal{O}((M_T N)^2 K T M_R)$, respectively. In Stage II, the dominant computation corresponds to a single rank-1 approximation, which has complexity $\mathcal{O}(M_T N T M_R)$. Then, the asymptotic complexity per iteration of the PAKRON receiver is $\max((M_T N)^2 I K, (M_T N)^2 K T M_R, M_T N T M_R)$. On the other hand, the computational complexity of the TALS-TUCKER receiver is dictated by steps 1, 2, and 3, which have complexities $\mathcal{O}((N)^2 I K T)$, $\mathcal{O}(I K M_R (M_T)^2)$, and $\mathcal{O}(K T M_R (M_T N)^2)$, respectively. Therefore, the asymptotical complexity of the TALS-TUCKER receiver is $\max((N)^2 I K T, I K M_R (M_T)^2, K T M_R (M_T N)^2)$. Table I summarizes the asymptotic complexities the identifiability conditions of our proposed receivers in comparison to competing methods. It is important to emphasize that BALS ([18]) is the simplest receiver and, consequently, generally exhibits the lowest computational complexity in terms of flops when compared with the BTKF, PAKRON, and TUCKER receivers. Moreover, as the number of BD-RIS scattering elements increases, the TUCKER receiver becomes less complex than the BTKF one, which by its turn, is less complex than PAKRON (although this gap noticeably narrows as N grows). Among all considered schemes, PAKRON usually incurs the highest flop count. Note, however, that the higher computational complexity of our

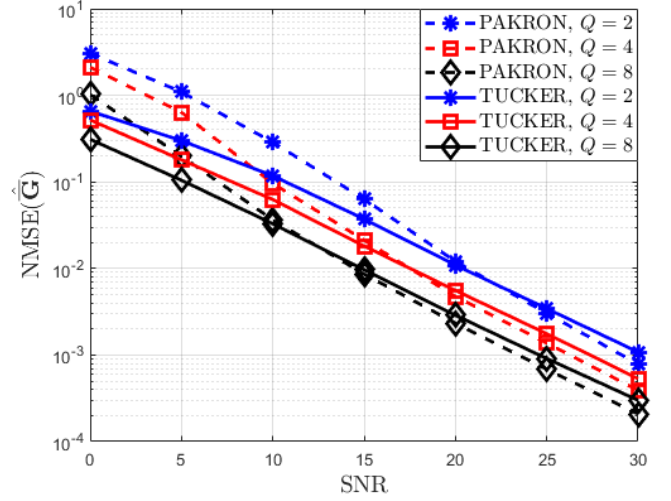


Fig. 6. NMSE performance of the user to the BD-RIS channels.

proposed methods comes with their ability to operate in semi-blindly without the need of pilot sequences.

V. SIMULATION RESULTS

In this section, we present several numerical experiments to evaluate the performance of our proposed semi-blind receivers under various setups. The channel estimation accuracy is evaluated in terms of normalized mean square error (NMSE), which is given by

$$\text{NMSE}(\hat{\mathbf{H}}) = \frac{1}{R} \sum_{r=1}^R \frac{\|\mathbf{\Xi}^{(r)} - \hat{\mathbf{\Xi}}^{(r)}\|_F^2}{\|\mathbf{\Xi}^{(r)}\|_F^2}, \quad (61)$$

where $\mathbf{\Xi} \in \{\mathbf{H}, \mathbf{G}\}$ and $\hat{\mathbf{\Xi}}^{(r)}$ is their estimate obtained in r -th Monte Carlo run. We also show numerical results in terms of the symbol error rate (SER) performance as a function of the signal to noise ratio (SNR) in dB. As references for comparison, we also plot the performance of competing (pilot-assisted) baseline methods, such as the LS-based channel estimation method proposed in [35], and the BTKF and BTALS methods proposed recently in [18]. The performance of the traditional zero-forcing receiver operating under perfect channel knowledge is also plotted. The results represent an average over $R = 1000$ Monte Carlo runs. Regarding the channel model, we consider the Rayleigh fading case (i.e., the entries of the channel matrices are independent and identically distributed zero-mean circularly symmetric complex Gaussian random variables) as well as a multipath (low-rank) geometrical channel model, where the path directions are randomly generated according to a uniform distribution. In this case, at each Monte Carlo run, the azimuth and elevation angles are drawn within the intervals $[-\pi/2, \pi/2]$ and $[0, \pi/2]$, respectively. The system parameters used in this analysis were $N = 16$, $M_R = 4$, $M_T = 2$, $I = 2$, $K = 32$, $T = 4$, and $Q \in \{2, 4, 8\}$.

Figures 6 and 7 illustrate the channel estimation accuracy PAKRON and TUCKER receivers. Let us first consider Figure 6, which depicts the performance of the estimated user to

Receiver	Complexity	Identifiability condition	Approach
PAKRON	$\max((M_T N)^2 I K, (M_T N)^2 K T M_R, M_T N T M_R)$	$K \geq \max\left(\frac{M_T N}{I}, \frac{M_T N}{T M_R}\right)$	Semi-Blind
TUCKER	$\max(N^2 I K T, I K M_R (M_T)^2, K T M_R (M_T N)^2)$	$K \geq \max\left(\frac{N}{I T}, \frac{M_T}{T M_R}, \frac{M_T N}{T M_R}\right)$	Semi-Blind
BTKF	$\max\left(M_R M_T \frac{N^2}{Q}, K \left(\frac{N^2}{Q}\right)^2\right)$ [18]	$K \geq \frac{N^2}{Q}$	Pilot-Assisted
BTALS	$\max\left(K M_T \left(\frac{N^2}{Q}\right)^2, K M_R \left(\frac{N^2}{Q}\right)^2\right)$ [18]	$K \geq \max\left(\frac{N}{M_T}, \frac{N}{M_R}\right)$	Pilot-Assisted

TABLE I
SUMMARY OF IDENTIFIABILITY CONDITIONS AND COMPUTATIONAL COMPLEXITY OF MAIN SOLUTIONS IN THE LITERATURE.

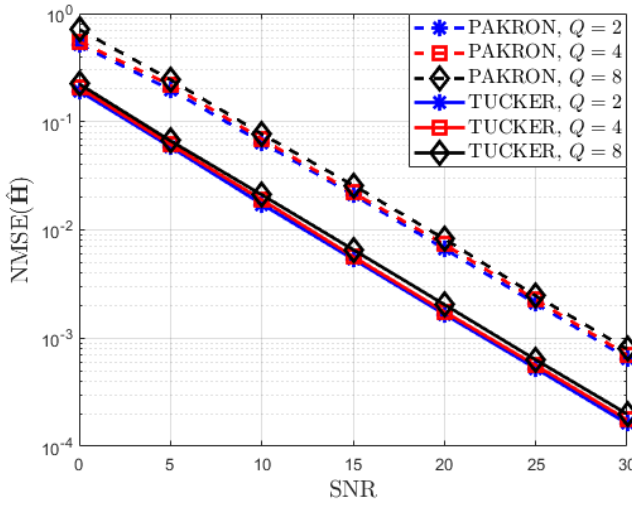


Fig. 7. NMSE performance of the user to the BD-RIS channels.

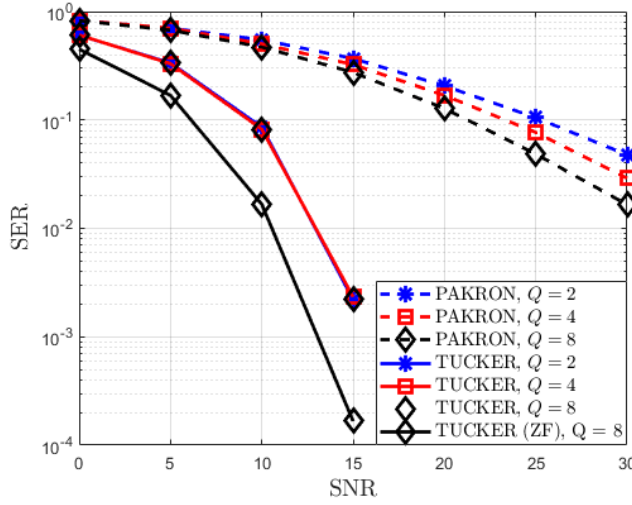


Fig. 8. SER performance of the proposed algorithm.

the BR-RIS channel (\bar{G}). It is noteworthy that the PAKRON receiver shows greater degradation than the TUCKER receiver at lower SNR levels (in particular until 10dB). However, in the higher SNR regime, this performance gap tends to diminish, resulting in nearly identical performances, with the PAKRON receiver showing a slight tendency to outperform the TUCKER

one. Moreover, we observe that both algorithms are sensitive to variations in the number of groups Q . This sensitivity is anticipated since the number of blocks can influence the iterative part of the PAKRON receiver, specifically the estimation of the channel \bar{G} and the structured matrix Ω . On the other hand, Figure 7 demonstrates that the TUCKER receiver consistently outperforms the PAKRON receiver across the entire SNR range. Nevertheless, both solutions show insensitivity to the number of groups. This can be explained by: (I) For the PAKRON receiver, the estimate of the channel \bar{H} is extracted by applying a Kronecker factorization to the Ω (stage II) matrix already estimated during the iterative part (stage I). This process reduces the sensitivity of the \bar{H} channel estimation concerning variations in the number of groups. However, there is error propagation from stage I to stage II, which explains the gap between the PAKRON and TUCKER receivers, thereby favoring the latter. In summary, PAKRON operates on a third-order tensor model whose factor matrices are constrained. This induces a coupling between the dimensions of the original tensor. As a consequence, it becomes more sensitive to changes in the number of groups and suffers a performance degradation in the estimation of channel \bar{G} at low SNR when compared with the TUCKER receiver. The TUCKER receiver, in contrast, preserves the fourth-order tensor structure of the received signal and thus does not incur diversity loss, since no dimension coupling occurs. As a result, it achieves more accurate estimates of \bar{G} in the low SNR regime. Nevertheless, this advantage tends to diminish as Q grows. For the channel \bar{H} , the TUCKER receiver also surpasses the PAKRON receiver in all simulated SNR range. This is mainly because it retains the diversity offered by the fourth-order tensor structure while enabling a single-stage processing, thereby avoiding the extra stage required by PAKRON. Such an additional stage leads to error propagation, which appears to be the primary reason for the performance disparity between the two receivers with respect to the estimation of the channel matrix \bar{H} .

The impact of this error propagation is also evident in Figure 8, where the TUCKER receiver significantly outperforms the PAKRON receiver, particularly with a higher-order 64-PSK constellation scheme. We also compare the TUCKER receiver with the clairvoyant zero-forcing (ZF) receiver derived directly from (44) that assumes perfect channel knowledge. The results indicate strong performance in comparison to the ideal channel scenario. Additionally, the performance difference stems from

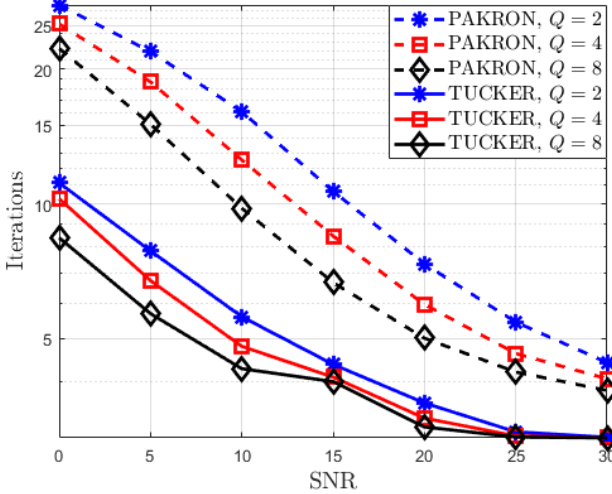


Fig. 9. Average number of iterations.

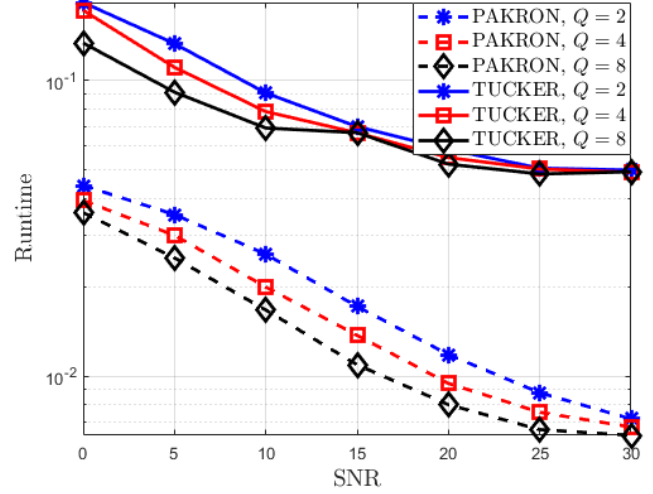


Fig. 10. Average runtime

the fact that, for the PAKRON receiver, the received signal tensor is reduced from a fourth-order to a third-order model. Due to this order reduction, the original tensor structure is lost, leading to mode mixing. This loss prevents the tensor structure from being fully exploited, a capability that the TUCKER receiver retains by maintaining the original tensor order.

The complexity of the proposed solution is evaluated using two key metrics: the average number of iterations required for convergence and the corresponding average runtime. These metrics are shown in Figures 9 and 10. The findings depicted in these figures are quite revealing. Notably, while the PAKRON algorithm requires more iterations to converge than the TUCKER algorithm, it achieves superior execution speed. This implies that PAKRON can complete more iterations within the same time period, suggesting more efficient use of computational cycles. Consequently, the TUCKER algorithm, despite having fewer iterations, is considered computationally more complex. This complexity arises from the different computational demands of the two algorithms. Specifically, PAKRON computes two pseudo-inverses, whereas TUCKER requires three. Given the high computational cost of calculating pseudo-inverses, especially as the dimensions of the problem matrices increase, it is evident that the TUCKER approach incurs higher computational cost.

In Figure 11, we present a compelling comparison of our algorithms against established works in the literature, specifically the innovative proposal in [11] and the advanced approach outlined in [45]. The author of [11] provides a conventional LS solution, while [45] and [18] introduce a sophisticated tensor approach, culminating in a closed-form solution known as LS-KRF [45], BTKF [18], and BTALS [18], for composite channel estimation. This one is characterized as a block Kronecker product between the involved channels, expressed as: $\mathbf{H}_C = \mathbf{H} \otimes \mathbf{G} = [\mathbf{H}^{(1)} \otimes \mathbf{G}^{(1)} \dots \mathbf{H}^{(Q)} \otimes \mathbf{G}^{(Q)}]$. Unlike our approach, which assumes the channel \mathbf{G} varies dynamically over time, the competitor's model assumes a quasi-static channel. To ensure a fair and rigorous comparison, the NMSE of our composite channel is calculated

as an average⁶ across I composite channels, where $\mathbf{H}_C^i = \mathbf{H}^i \otimes \mathbf{G}_i$ for $i = 1, \dots, I$. Considering the setup $M_R = 10$, $M_T = 2$, $K = 32$, $I = 4$, $T = 8$, $N = 16$ and an i.i.d channel model, our proposed solutions, the TUCKER and PAKRON receivers, demonstrate good performance, both significantly outperforming the LS method described in [11]. This outcome is expected, given that the LS solution's simplicity fails to leverage the intrinsic tensor structure of the signal model. In contrast, our approach leverages this structure to achieve noise-rejection gain. Moreover, while the competitor receiver analyzed in [45] and [18] deliver superior results, this is understandable since both our method and the competitor algorithms benefit from effective noise rejection. However, our semi-blind receivers necessitate the estimation of three matrices (\mathbf{H} , $\bar{\mathbf{G}}$, and \mathbf{X}), compared to LS-KRF, BTALS, and BTKF receivers which are limited to estimating the first two. Nevertheless, the proposed semi-blind methods also delivers early estimates of the data symbols, in contrast to the competing methods which do not have this feature, requiring a dedicated pilot transmission period prior to symbol decoding.

Remark 4: The outcomes are influenced by the designs of matrices \mathbf{P} and \mathbf{W} , and consequently by Ψ . We focus on the design outlined in Section II-A. It is essential to note that the optimal design of the rotation matrix \mathbf{P} and the coding matrix $\bar{\mathbf{W}}$ can significantly impact the results. However, exploring this aspect is beyond the scope of this paper.

VI. CONCLUSION

In this paper, we proposed a novel tensor-based semi-blind receiver design for BD-RIS-assisted multiple-input multiple-output (MIMO) communication systems, where we assume a time-varying UT-intelligent reconfigurable surface (IRS) channel, which leads us to a fourth-order PARATUCK tensor model for the received signals. Exploiting this, we

⁶An alternative approach could involve considering $I = 1$, but this scenario falls within the framework addressed in our conference version

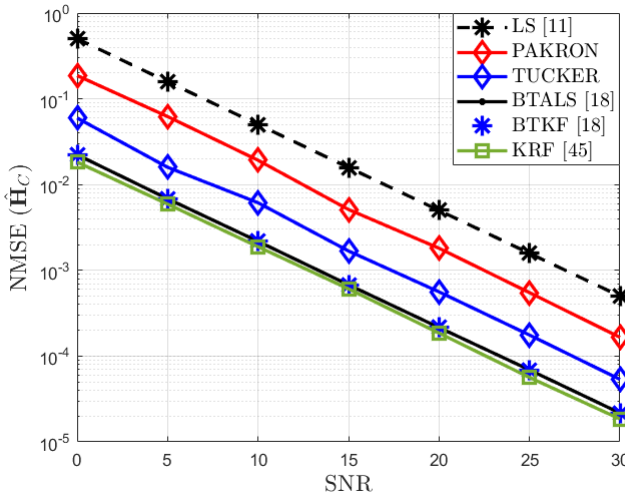


Fig. 11. NMSE performance of the composed channel in comparison with the literature works.

formulated a semi-blind receiver that is a data-aided channel estimator, avoiding the use of pilot sequences, while jointly estimating the BD-RIS-BS channel, the UT-BD-RIS channel, and the transmitted symbols. Specifically, we proposed to the recipients: I) The PAKRON receiver (Algorithm 1) is a two-stage approach where, first, the data symbols are estimated jointly with a structured matrix Ω which is composed by the Kronecker product between the BD-RIS-BS and the data matrix symbols in an iterative way by means of a BALS. Next, in the second stage, a Kronecker factorization is applied on the estimated version of the Ω to estimate the BD-RIS-BS channel component as well as the symbols. II) The TUCKER receiver is a fourth-order tensor decomposition method, where the channel and the data are jointly and iteratively estimated in a single stage via an TALS algorithm (4).

Our results indicate that the TUCKER receiver is more efficient than the PAKRON receiver in terms of channel estimation and data symbol accuracy. However, it is more computationally complex than PAKRON. Additionally, both of our methods outperform the competing method LS, as it does not exploit the inherent multidimensional structure of the received signal. On the other hand, the competing method LS-KRF⁷ exploit the tensor structure to surpass our proposed method. However, the competing method is a pilot-assisted scheme, whereas our approach is a semi-blind scheme suitable for scenarios with limited or unavailable pilot resources. A possible hybrid implementation of the proposed semi-blind receiver uses the soft estimates of the data symbol matrix delivered by PAKRON as an initialization for the TUCKER receiver. Another perspective of this work is to investigate the optimal design of the matrix Ψ . Additionally, new tensor structures as well as the Cramér-Rao bound can be derived for the different receivers.

REFERENCES

- [1] C. Pan, H. Ren, K. Wang, J. F. Kolb, M. Elkashlan, M. Chen, M. Di Renzo, Y. Hao, J. Wang, A. L. Swindlehurst, X. You, and L. Hanzo, “Reconfigurable intelligent surfaces for 6G systems: Principles, applications, and research directions,” *IEEE Commun. Mag.*, vol. 59, no. 6, pp. 14–20, 2021.
- [2] S. Basharat, S. A. Hassan, H. Pervaiz, A. Mahmood, Z. Ding, and M. Gidlund, “Reconfigurable intelligent surfaces: Potentials, applications, and challenges for 6G wireless networks,” *IEEE Wireless Commun.*, vol. 28, no. 6, pp. 184–191, 2021.
- [3] X. Yuan, Y.-J. A. Zhang, Y. Shi, W. Yan, and H. Liu, “Reconfigurable-intelligent-surface empowered wireless communications: Challenges and opportunities,” *IEEE Wireless Commun.*, vol. 28, no. 2, pp. 136–143, 2021.
- [4] G. C. Alexandropoulos, N. Shlezinger, I. Alamzadeh, M. F. Imani, H. Zhang, and Y. C. Eldar, “Hybrid reconfigurable intelligent metasurfaces: Enabling simultaneous tunable reflections and sensing for 6G wireless communications,” *IEEE Veh. Technol. Mag.*, vol. 19, no. 1, pp. 75–84, 2024.
- [5] H. Zhang, N. Shlezinger, G. C. Alexandropoulos, A. Shultzman, I. Alamzadeh, M. F. Imani, and Y. C. Eldar, “Channel estimation with hybrid reconfigurable intelligent metasurfaces,” *IEEE Trans. Commun.*, vol. 71, no. 4, pp. 2441–2456, 2023.
- [6] A. L. Magalhães and A. L. F. de Almeida, “Joint channel and symbol estimation for hybrid RIS wireless communications,” in *(ISWCS)*, 2024, pp. 1–6.
- [7] Z. Wang, X. Mu, J. Xu, and Y. Liu, “Simultaneously transmitting and reflecting surface (STARS) for terahertz communications,” *IEEE J. Sel. Topics Signal Process.*, vol. 17, no. 4, pp. 861–877, 2023.
- [8] X. Zhai, G. Han, Y. Cai, Y. Liu, and L. Hanzo, “Simultaneously transmitting and reflecting (STAR) RIS assisted over-the-air computation systems,” *IEEE Trans. Commun.*, vol. 71, no. 3, pp. 1309–1322, 2023.
- [9] Y. Liu, X. Mu, J. Xu, R. Schober, Y. Hao, H. V. Poor, and L. Hanzo, “STAR: Simultaneous Transmission and Reflection for 360° Coverage by Intelligent Surfaces,” *IEEE Wireless Commun.*, vol. 28, no. 6, pp. 102–109, 2021.
- [10] H. Li, S. Shen, and B. Clerckx, “Beyond diagonal reconfigurable intelligent surfaces: From transmitting and reflecting modes to single-, group-, and fully-connected architectures,” *IEEE Trans. Wireless Commun.*, vol. 22, no. 4, pp. 2311–2324, 2023.
- [11] H. Li, S. Shen, Y. Zhang, and B. Clerckx, “Channel estimation and beamforming for beyond diagonal reconfigurable intelligent surfaces,” *IEEE Trans. Signal Process.*, vol. 72, pp. 3318–3332, 2024.
- [12] Q. Li, M. El-Hajjar, I. Hemadeh, A. Shojaeifard, A. A. M. Mourad, B. Clerckx, and L. Hanzo, “Reconfigurable intelligent surfaces relying on non-diagonal phase shift matrices,” *IEEE Trans. Vehicular Tech.*, vol. 71, no. 6, pp. 6367–6383, 2022.
- [13] S. Shen, B. Clerckx, and R. Murch, “Modeling and architecture design of reconfigurable intelligent surfaces using scattering parameter network analysis,” *IEEE Trans. Wireless Commun.*, vol. 21, no. 2, pp. 1229–1243, 2022.
- [14] M. Nerini, S. Shen, H. Li, M. Di Renzo, and B. Clerckx, “A universal framework for multiport network analysis of reconfigurable intelligent surfaces,” *IEEE Trans. Wireless Commun.*, vol. 23, no. 10, pp. 14 575–14 590, 2024.
- [15] M. Nerini, S. Shen, and B. Clerckx, “Closed-form global optimization of beyond diagonal reconfigurable intelligent surfaces,” *IEEE Trans. Wireless Commun.*, vol. 23, no. 2, pp. 1037–1051, 2024.
- [16] M. Soleymani, I. Santamaría, E. Jorswieck, and B. Clerckx, “Optimization of rate-splitting multiple access in beyond diagonal RIS-assisted urllc systems,” *IEEE Trans. Wireless Commun.*, pp. 1–1, 2023.
- [17] B. Zheng, C. You, W. Mei, and R. Zhang, “A survey on channel estimation and practical passive beamforming design for intelligent reflecting surface aided wireless communications,” *IEEE Commun. Surveys Tuts.*, vol. 24, no. 2, pp. 1035–1071, Feb. 2022.
- [18] A. L. F. de Almeida, B. Sokal, H. Li, and B. Clerckx, “Channel estimation for beyond diagonal RIS via tensor decomposition,” *IEEE Trans. Signal Process.*, 2025.
- [19] G. T. de Araújo and A. L. F. de Almeida, “Semi-blind channel estimation for beyond diagonal ris,” in *2024 58th Asilomar Conference on Signals, Systems, and Computers*, 2024, pp. 1586–1590.
- [20] G. T. de Araújo, A. L. F. de Almeida, R. Boyer, and G. Fodor, “Semi-blind joint channel and symbol estimation for IRS-assisted MIMO systems,” *IEEE Trans. Sig. Proces.*, vol. 71, pp. 1184–1199, 2023.

⁷The same for BTKF and BTALS in [18].

[21] A. L. F. de Almeida, G. Favier, and J. C. M. Mota, "PARAFAC-based unified tensor modeling for wireless communication systems with application to blind multiuser equalization," *Signal Processing*, vol. 87, no. 2, pp. 337–351, 2007, tensor Signal Processing.

[22] A. L. F. de Almeida, G. Favier, and J. C. M. Mota, "A constrained factor decomposition with application to mimo antenna systems," *IEEE Trans. Signal Process.*, vol. 56, no. 6, pp. 2429–2442, 2008.

[23] G. Favier and A. L. F. de Almeida, "Tensor space-time-frequency coding with semi-blind receivers for MIMO wireless communication systems," *IEEE Trans. Signal Process.*, vol. 62, no. 22, pp. 5987–6002, 11 2014.

[24] L. R. Ximenes, G. Favier, and A. L. F. de Almeida, "Semi-blind receivers for non-regenerative cooperative mimo communications based on nested parafac modeling," *IEEE Trans. Signal Process.*, vol. 63, no. 18, pp. 4985–4998, 2015.

[25] L. R. Ximenes, G. Favier, A. L. F. de Almeida, and Y. C. B. Silva, "PARAFAC-PARATUCK semi-blind receivers for two-hop cooperative MIMO relay systems," *IEEE Trans. Sig. Proces.*, vol. 62, no. 14, pp. 3604–3615, 2014.

[26] H. Chen, F. Ahmad, S. Vorobyov, and F. Porikli, "Tensor decompositions in wireless communications and mimo radar," *IEEE J. Sel. Topics Signal Process.*, vol. 15, no. 3, pp. 438–453, 2021.

[27] Fazal-E-Asim, B. Sokal, A. L. F. de Almeida, B. Makki, and G. Fodor, "Structured channel estimation for RIS-assisted THz communications," *IEEE Trans. Veh. Technol.*, pp. 1–6, 2024.

[28] Fazal-E-Asim, A. L. F. De Almeida, B. Sokal, B. Makki, and G. Fodor, "Two-dimensional channel parameter estimation for IRS-assisted networks," *IEEE Trans. Commun.*, pp. 1–1, 2024.

[29] Y. S. Ribeiro, A. L. F. de Almeida, Fazal-E-Asim, B. Makki, and G. Fodor, "Low-complexity joint active and passive beamforming design for IRS-assisted MIMO," *IEEE Wireless Commun. Lett.*, vol. 13, no. 3, pp. 607–611, 2024.

[30] B. Sokal, P. R. B. Gomes, A. L. F. de Almeida, B. Makki, and G. Fodor, "Reducing the control overhead of intelligent reconfigurable surfaces via a tensor-based low-rank factorization approach," *IEEE Trans. Wireless Commun.*, vol. 22, no. 10, pp. 6578–6593, 2023.

[31] G. T. de Araújo, A. L. F. de Almeida, and R. Boyer, "Channel estimation for intelligent reflecting surface assisted MIMO systems: A tensor modeling approach," *IEEE J. Sel. Topics Signal Process.*, vol. 15, no. 3, pp. 789–802, Apr 2021.

[32] P. R. B. Gomes, G. T. d. Araújo, B. Sokal, A. L. F. d. Almeida, B. Makki, and G. Fodor, "Channel estimation in RIS-assisted MIMO systems operating under imperfections," *IEEE Trans. Veh. Technol.*, pp. 1–14, 2023.

[33] S. Gherekhloo, K. Ardah, A. L. F. De Almeida, M. Maleki, and M. Haardt, "Nested parafac tensor-based channel estimation method for double RIS-aided mimo communication systems," in *(EUSIPCO)*, 2023, pp. 1674–1678.

[34] G. C. Nwalozie, A. L. de Almeida, and M. Haardt, "Enhanced channel estimation for double RIS-aided mimo systems using coupled tensor decompositions," *Signal Processing*, vol. 234, p. 109979, 2025.

[35] H. Li, Y. Zhang, and B. Clerckx, "Channel estimation for beyond diagonal reconfigurable intelligent surfaces with group-connected architectures," in *(CAMSAP)*, 2023, pp. 21–25.

[36] G. Favier and A. de Almeida, "Overview of constrained PARAFAC models," *EURASIP J. Adv. Signal Process.*, 2014.

[37] R. A. Harshman, "Foundations of the PARAFAC procedure: Models and conditions for an "explanatory" multi-modal factor analysis," *UCLA Working Papers in Phonetics*, vol. 16, pp. 1–84, 1970.

[38] C. Eckart and G. Young, "The approximation of one matrix by another of lower rank," *Psychometrika*, vol. 1, no. 3, pp. 211–218, Sep 1936.

[39] B. Sokal, A. L. de Almeida, and M. Haardt, "Semi-blind receivers for mimo multi-relaying systems via rank-one tensor approximations," *Signal Processing*, vol. 166, p. 107254, 2020.

[40] A. Stegeman and N. D. Sidiropoulos, "On Kruskal's uniqueness condition for the candecomp/parafac decomposition," *Linear Algebra and its Applications*, vol. 420, no. 2, pp. 540 – 552, 2007.

[41] N. D. Sidiropoulos and R. Bro, "On the uniqueness of multilinear decomposition of n-way arrays," *Journal of Chemometrics*, vol. 14, no. 3, pp. 229–239, 2000.

[42] A. Stegeman and N. D. Sidiropoulos, "On kruskal's uniqueness condition for the CANDECOMP/PARAFAC decomposition," *Linear Algebra and its Applications*, vol. 420, no. 2, pp. 540 – 552, 2007.

[43] L. De Lathauwer, "Decompositions of a higher-order tensor in block terms—part I: Lemmas for partitioned matrices," *SIAM Journal on Matrix Analysis and Applications*, vol. 30, no. 3, pp. 1022–1032, 2008.

[44] P. M. R. de Oliveira, C. A. R. Fernandes, G. Favier, and R. Boyer, "PARATUCK semi-blind receivers for relaying multi-hop MIMO systems," *Digital Signal Processing*, vol. 92, pp. 127 – 138, 2019.

[45] B. Sokal, Fazal-E-Asim, A. L. F. de Almeida, H. Li, and B. Clerckx, "A decoupled channel estimation method for beyond diagonal RIS," in *2024 58th Asilomar Conference on Signals, Systems, and Computers*, 2024, pp. 1395–1399.